

Effects of bath pH on structural and electrochemical performance of Cu₂O

Guangli Li¹ · Yaohan Huang¹ · Qingfei Fan¹ · Meili Zhang¹ · Qi Lan¹ · Ximei Fan¹ · Zuowan Zhou¹ · Chaoliang Zhang²

Received: 30 November 2015 / Revised: 11 April 2016 / Accepted: 9 May 2016 / Published online: 13 June 2016
© Springer-Verlag Berlin Heidelberg 2016

Abstract Well-defined cuprous oxides (Cu₂O) with different morphologies were successfully deposited on fluorine-doped tin oxide (FTO)-covered glass substrates by potentiostatic deposition. The effect of the pH values on the crystal morphologies of Cu₂O was studied. The as-prepared products were characterized by means of X-ray diffraction (XRD), scanning electron microscopy (SEM), linear sweep voltammetry (LSV), electrochemical impedance spectroscopy (EIS), and UV-visible spectroscopy. The typical XRD patterns revealed that all Cu₂O thin films were pure Cu₂O phase. Different crystal morphologies of Cu₂O could be obtained by varying pH. The Cu₂O thin film was composed of a large number of star-like shape grains with the pH of 4.8. With a further increase of the pH, the Cu₂O film showed the uniform dendrite morphology. LSV uncovered that E_R (reduction potential of Cu²⁺ to Cu⁺) increased with the pH value enlargement. According to the EIS, diffusion coefficient of Cu²⁺ ion was reduced with the increase of the pH. The UV-vis absorption spectra revealed that the broad absorption peaks were from 300 to 500 nm and the evaluated band gap of the films was tunable in the range of 2.02–2.67 eV, with the variation of the pH values. According to the experiment and relevant literatures, the probable electrodeposition mechanism of the Cu₂O was discussed.

Keywords Cu₂O films · Potentiostatic deposition · Diffusion coefficient · pH

Introduction

As a non-stoichiometric semiconductor [1], with a direct band gap around 2.09 eV, cuprous oxide (Cu₂O) has advantages of good gas sensitivity, non-toxicity, and low costs. Therefore, it is widely used in solar cells, gas sensors, magnetic storage, lithium ion batteries, biological sensors, microdevices, and negative electrodes [2–9]. The utilization efficiency of sunlight by Cu₂O thin films can reach 20 % in theory [10], so most of research work has been done in solar energy conversion. However, the present report on the highest energy conversion efficiency is only 2.1 % [11], whose main reason is that it is difficult to control Cu₂O surface morphology, particle size, and other semiconducting properties.

So far, many deposited methods have been intensively focused on the synthesis of Cu₂O with a variety of morphologies, such as thermal oxidation [12], chemical vapor deposition [13], reactive sputtering [14], wet chemical reduction [15–17], chemical oxidation [18], electrodeposition [19–24], and so on. Among these techniques, electrodeposition is one of the most attractive ways to manufacture semiconductor oxide films over conductive substrates. It provides advantages such as the ability to use a low costs, low synthesis temperature, and large area deposition. Also, the thickness and morphology of the films can be controlled by adjusting the parameters such as the additive, substrate, electrolyte concentration, solution temperature, pH, and so on [25–28].

Shao et al. [29] reported the electrochemical deposition of Cu₂O microcrystals on the FTO glass substrates. When varying the bath pH, Cu₂O nanocrystalline changed from dendritic structure to quasi-cuboid structure. Paracchino et al. [7]

✉ Ximei Fan
fanximei@126.com

¹ Key Laboratory of Advanced Technologies of Materials, Ministry of Education of China, School of Materials Science and Engineering, Southwest Jiaotong University, Chengdu 610031, People's Republic of China

² State Key Laboratory of Oral Diseases, West China Hospital of Stomatology, Sichuan University, Chengdu, Sichuan 610041, China

studied the effects of solution temperature, pH, and deposition current density on the photoelectrochemical properties of Cu_2O , and they found that the highest photocurrent obtained was -2.4 mA cm^{-2} at 0.25 V vs. reversible hydrogen electrode (RHE) for a film thickness of 1.3 μm .

According to the above, we can draw a conclusion that the deposition conditions play an important part in the microstructure and properties of Cu_2O thin films. The bath pH can also affect the shape formation of crystals in various ways [30]. Its effect can interfere with diffusion limited growth. In this paper, a series of Cu_2O films were electrodeposited using cupric acetate solutions with bath pH ranging from 4.8 to 5.8. The effects of bath pH on the morphological, microstructural, and electrochemical properties of the as-deposited Cu_2O films were investigated in detail.

Experiment section

Materials

All of the chemical reagents were analytical grade and used without further purification. All the solutions in this study were prepared from deionized water which was further purified by a Millipore Milli-Q purification system (resistivity $\geq 18.2 \text{ M}\Omega\cdot\text{cm}$). Fluorinated tin oxide-covered glass substrates ($10 \text{ }\Omega\cdot\text{cm}^{-2}$, Xiang Town Technologies Ltd., China) were used as substrates and cleaned in four 10-min steps of cleaning in ultrasonicated acetone, ethanol, 1:1 H_2O_2 /ammonia, and finally ultrapure water.

Preparation of Cu_2O films

The electrodeposition was performed on a IM6 electrochemical workstation (Zahner, GER). Growth of Cu_2O particles was carried out in a conventional three-electrode cell equipped with a carbon rod as the counter electrode and a saturated calomel electrode (SCE) as the reference electrode. The working electrode was a FTO glass with a surface area of $30 \times 20 \text{ mm}^2$ exposed to the electrolyte. The electrolytes are 0.02 M $\text{Cu}(\text{Ac})_2$ and 0.1 M NaAc aqueous solution. The pH values of the electrolytes were modulated by adding acetic acid. The temperature of the electrolytes was maintained at 50 °C during the experiments. Electrodeposition was carried out under potentiostatic condition of -250 mV against the SCE for 300 s. The samples are deposited in the acidic electrolyte system. If the acidity is too strong, such as the pH smaller than 4, H^+ would prompt Cu_2O into Cu. When the pH is too high, such as the pH more than 6, it is difficult to deposit Cu_2O on the conductive glass. Therefore, the samples were prepared at different bath pH (4.8, 5.0, 5.2, 5.4, 5.6, and 5.8). After deposition, the films were rinsed with copious amounts of double-distilled water, dried at room temperature.

Characterization

To determine the phase of the products, the crystallographic properties were carried out on a Philips X'Pert PRO X-ray diffractometer, using Cu $\text{K}\alpha$ radiation, at a scanning rate of $2^\circ/\text{min}$ in the 2θ range of $20\text{--}65^\circ$. The surface morphology of the Cu_2O thin films were observed by scanning electron microscopy (SEM, Fei Quanta 200, USA). The transmission spectra of the thin films were measured with a UV-2550 UV-vis spectrophotometer (Shimadzu, Japan) ranging from 300 to 650 nm.

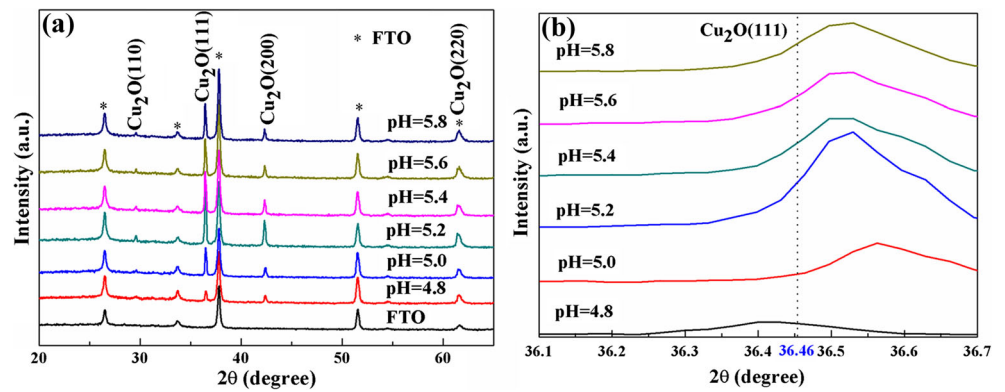
The electrochemical properties of the deposited samples were characterized by linear sweep voltammogram (LSV) and electrochemical impedance spectroscopy (EIS) performed on an IM6 electrochemical workstation system. The LSV measurements were performed in an aqueous solution of 0.1 M sodium acetate and 0.02 M cupric acetate with different pH in a standard three-electrode configuration coupled with the FTO (working electrode), a saturated calomel electrode (reference electrode), and a carbon rod (counter electrode). The EIS measurements were performed in an aqueous solution of 0.1 M sodium acetate and 0.02 M cupric acetate with different pH in a standard three-electrode configuration coupled with the sample films (working electrode), a saturated calomel electrode (reference electrode), and a carbon rod (counter electrode). The LSV measurements were operated at $10 \text{ mV}\cdot\text{s}^{-1}$ between -0.8 and 0.2 V (vs. SCE), and the EIS analyses were performed at the amplitude of 5 mV and at the frequency from 10 mHz to 100 kHz.

Results and discussion

Structural characterization of Cu_2O thin films

The XRD patterns for Cu_2O thin films deposited on FTO conductive glass with different pH values are shown in Fig. 1. From Fig. 1a, no impurities such as cupric oxides are found in the XRD pattern besides the substrate, which means that single-phase Cu_2O crystals can be obtained through electrodeposition method in this system. Figure 1b displays the enlarged peaks corresponding to (111) for Cu_2O samples. According to JCPDS card No. 78-2076, the diffraction peak appearing at $2\theta = 36.46^\circ$ corresponds to the (111) plane of cubic Cu_2O . The diffraction peak (111) shifted toward the region of small theta when the pH value was 4.8. According to Bragg equation, $2d\sin\theta = n\lambda$ (where d is the lattice plane distance value, θ the value of diffraction theta, and λ the wavelength of X-ray), it is obvious that as θ turns to be smaller, d will become larger accordingly. It indicated the crystalline lattice inflation. When the pH was greater than 4.8, the diffraction peak (111) shifted toward the region of larger theta

Fig. 1 **a** XRD patterns for Cu₂O thin films deposited on FTO conductive glass with different pH values and **b** corresponding enlarged (111) peaks



and *d* turns to be smaller which lead to the crystalline lattice contraction.

To determine the preferred orientation of the Cu₂O films, the intensity ratio I(111)/I(200) for the two most intense peaks is plotted as a function of the pH, and it is shown in Fig. 2. The relative ratio I(111)/I(200) value corresponding to a polycrystalline pure Cu₂O sample without preferential orientation is indicated by a solid horizontal line, and it has a value of 2.88. Hence, if the ratio is smaller than 2.88, the Cu₂O films deposited are formed in a [100] preferred orientation. Otherwise, the films reveal a [111] texture [31, 32]. Thus, it can be seen that pure Cu₂O films as-prepared displayed a [100] preferential orientation. This is maybe caused by anisotropic growth of the dendritic crystal films [33].

Surface morphology analysis

SEM images of Cu₂O crystals deposited at *E* = −0.25 V for 5 min in solutions containing 0.02 M copper acetate and 0.1 M sodium acetate at pH changing from 4.8 to 5.8 modulated with acetic acid are shown in Fig. 3.

It can be seen from Fig. 3a that particles of Cu₂O with star-like shape are dispersed on FTO and the grain sizes are heterogeneous. The Cu₂O crystalline grains are not completely covered on FTO conductive glass. When the pH increases to 5.0, the crystal particles developed along the apexes of the star-like morphology and many different branches were formed over a large area of the FTO (see Fig. 3b). With a further increase of the pH to 5.2–5.4, we found that the degree of branching gradually increased and more pronounced multiple branches were observed and formed a physically continuous crystal body (see Fig. 3c, d), which is consistent with the results reported by Jinbo Xue [34]. At a higher pH of 5.6–5.8, smaller grain size and dendrites were observed (Fig. 3e, f) and the dendrite morphology Cu₂O film was compact on the upper part of FTO. The results indicate that the morphologies of the Cu₂O films can be affected by the pH in electrolyte.

The EDX of Cu₂O film deposited at *E* = −0.25 V for 5 min in solution containing 0.02 M copper acetate and 0.1 M sodium acetate at a pH of 4.8 is shown in Fig. 4a. We can see the elements of Cu, O, Sn, and Ca in the EDX. Sn and Ca elements are from the conductive layer and the glass layer. According to the analysis of XRD and EDX, we can determine that the thin film is Cu₂O. Figure 4b is the macroscopic image of the Cu₂O obtained at a pH of 4.8. The entire substrates really covered by Cu₂O.

According to the relevant literatures and in combination with our experimental phenomenon, the possible formation process of the Cu₂O thin films is proposed as follows. Electrodeposition of Cu₂O involves two steps: the first step is reduction of Cu²⁺ ions to Cu⁺ ions (Eq. (R1)) and the second step is precipitation of Cu⁺ ions to Cu₂O on the working electrode. (Eq. (R2)) [34, 35]:

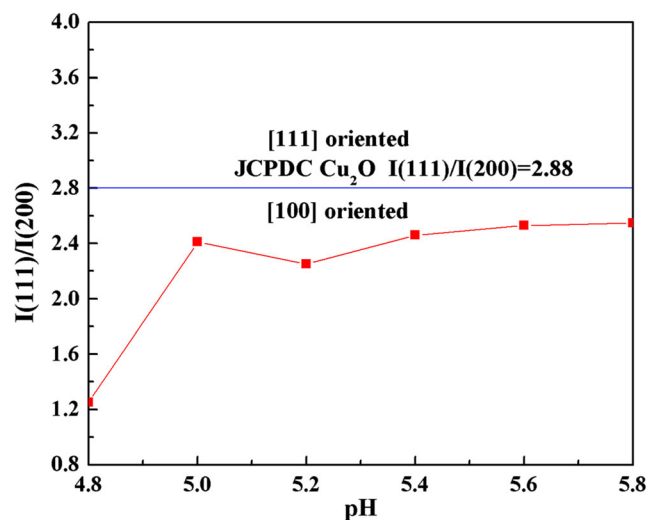
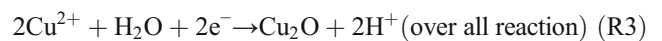
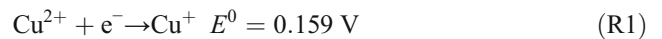
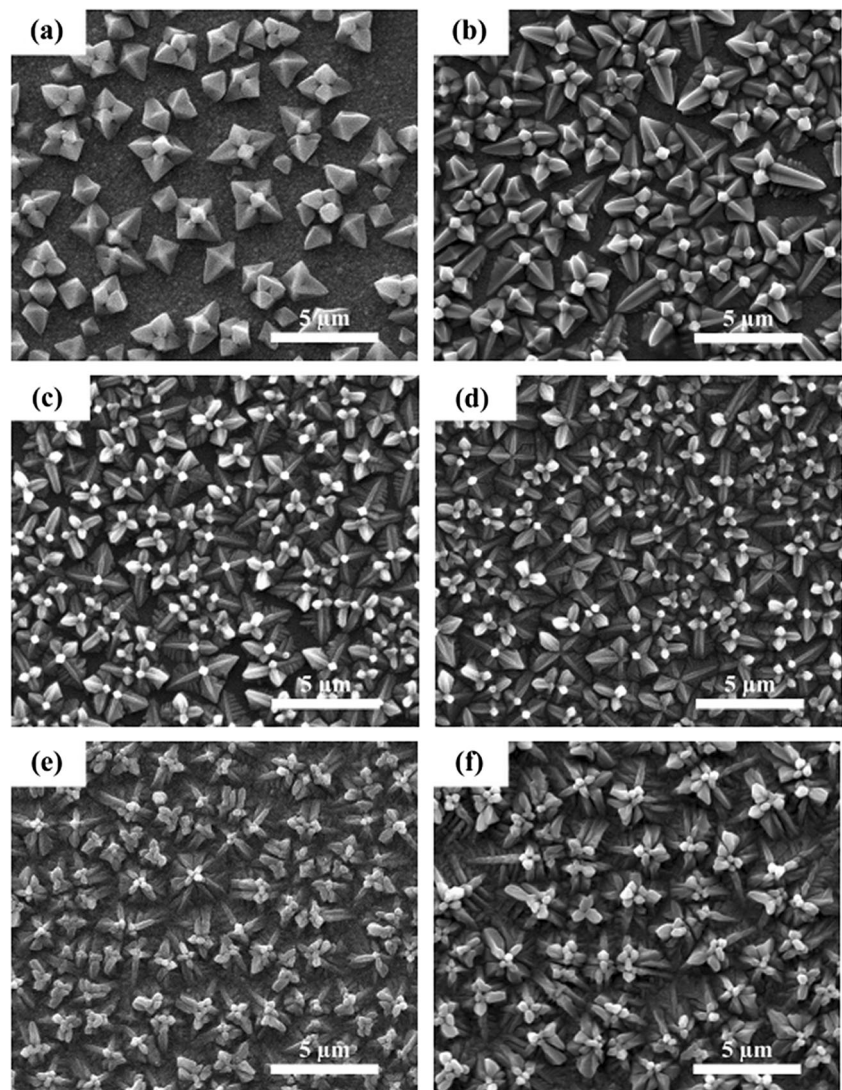


Fig. 2 Plot line of relative intensity I(111)/I(200) of X-ray diffraction peaks as a function of pH

Fig. 3 SEM images of Cu_2O films obtained at -0.25 V vs. SCE for 5 min in solutions containing 0.02 M copper acetate and 0.1 M sodium acetate at different pH values **a** pH = 4.8, **b** pH = 5.0, **c** pH = 5.2, **d** pH = 5.4, **e** pH = 5.6, and **f** pH = 5.8. *Insert:* vertical images of the Cu_2O films



The overpotential was generated for the cathodic deposition of Cu_2O when a deposition potential was more negative than the reduction potential of Cu^{2+} to Cu^+ ions (Eq. (R1)). The overpotential (η) is defined as the difference between the deposition potential (E_D) and the reduction potential (E_R) [36–38]:

$$\eta = |E_D - E_R| \quad (1)$$

The reduction potential of Cu^{2+} to Cu^+ is described by the Nernst equation [37]:

$$E_R = E^0 - 2.303 \frac{RT}{nF} \log_{10} \frac{[\text{Cu}^+]}{[\text{Cu}^{2+}]} \quad (2)$$

where $E^0 = 0.159$ V and $2.303RT/nF = 0.05916$ V at $T = 298.15$ K for the $\text{Cu}^{2+}/\text{Cu}^+$ redox couple. The solubility of Cu^+ ions in an aqueous solution at $T = 323.15$ K is [36]

$$\log_{10}[\text{Cu}^+] = -0.84 - \text{pH} \quad (3)$$

Thus, Eq. (2) at $T = 323.15$ K is reduced to

$$E_R = 0.1051 + 0.06412 \log_{10}[\text{Cu}^{2+}] + 0.6412 \text{pH} \quad (4)$$

Therefore, the overpotential for Eq. (R1) is controlled by several factors including the deposition potential, solution pH, solution temperature, and concentration of Cu^{2+} in the solution. In this paper, we make sure that electrodeposition potential and electrodeposition temperature remained unchanged. According to Eq. (4), the reduction is determined by pH of the solution and the concentration of Cu^{2+} ion at the interfacial region. Since the concentration of Cu^{2+} precursor is constant, E_R is linear correlation with the pH values [34]. In our experiment, E_D is constant. Therefore, we can come to a conclusion that a larger overpotential (η) is established at higher solution pH, which is consistent with the discovery of Han et al. [39]. According to Eq. (3) and Eq. (R1), the high solubility of Cu^+ ions at low pH values (<5.0) allows more Cu^{2+} ions to present in solution and promote the mass transport. Meanwhile, under

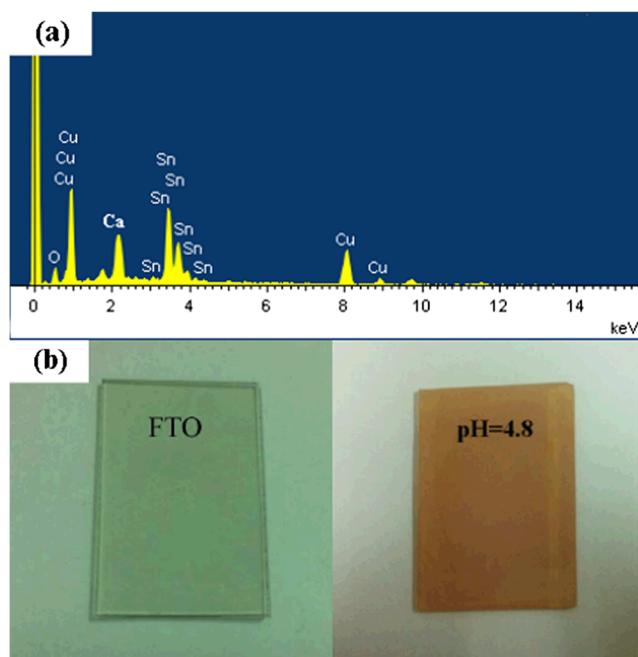


Fig. 4 **a** The EDX analysis of the Cu₂O film and **b** the macroscopic images of Cu₂O film obtained at -0.25 V vs. SCE for 5 min in a solution containing 0.02 M copper acetate and 0.1 M sodium acetate at a pH of 4.8

the low pH, the reduction rate of Cu²⁺ ions is relatively slow and the consumption of Cu²⁺ ions at the interface can be quickly compensated by mass transport [40]. Under these conditions, crystals grow surrounded by sufficient Cu²⁺ ions and are allowed to form a shape that can reach a minimum surface energy, so faceted shapes were obtained. With the increase of pH, the increased overpotential facilitated the nucleation process in the electrodeposition. Cu²⁺ ions were consumed faster than the transport rate of Cu²⁺ ions to the interfacial region, so the concentration of Cu²⁺ ions were very low at the interface, which created a depletion zone around the growing Cu₂O crystal [40, 41]. Once the depletion layer is formed, the apexes of a polyhedral crystal protrude further into the region of higher concentration and they can grow faster than the central parts of the facets; thus, dendritic branches are formed [34, 37, 40]. Therefore, branched crystals were produced at large pH because of the limitation of the transportation of Cu²⁺ ions (Fig. 3b). In this case, the degree of branching was expected to become more pronounced as the pH increases (Fig. 3c, d) [33]. When the pH reached 5.6 and 5.8, the primary branches of the dendrite grew together to form a surface coverage on the FTO and secondary branches of the dendrite were developed on the primary ones. In addition, the solubility of Cu²⁺ ions was extremely limited at high pH values, and Cu²⁺ ions rapidly precipitated out of solution as soon as they were generated electrochemically, which meant that they would quickly crystallize even if the morphology were not thermodynamically favorable (such as formation of branches).

Electrochemical properties

To better understand the relationship between reduction potential and pH values, the linear sweep voltammograms of Cu₂O were further applied for studying the reduction potential of the cathode. The RHE scale compensates for pH and would be more helpful in the discussions vs. the pH-sensitive SCE scale. Therefore, we referenced the potential to the RHE. RHE was converted through the following relationship [42].

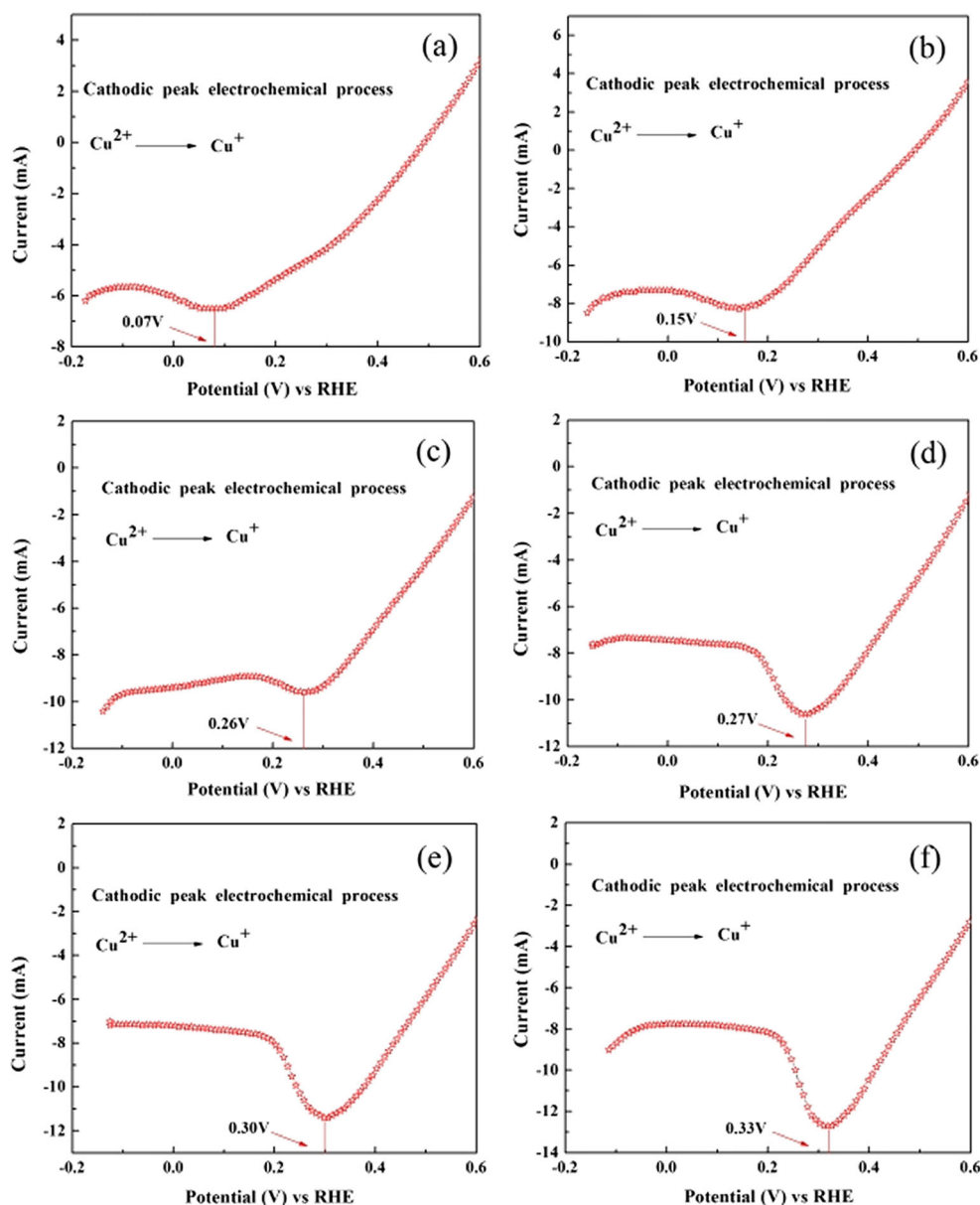
$$E(RHE) = E(SCE) + 0.0591pH + 0.24 \quad (5)$$

Figure 5 shows the linear sweep voltammograms of Cu₂O films electrodeposited on FTO at room temperature. The scan was performed in the cathodic direction. The cathodic peak is associated with the Cu(II) to Cu(I) restored (chemical equation in Fig. 4). It can be observed that as the pH values varied from 4.8 to 5.8, the reduction potential peak increased from 0.07 V to 0.33 V. An increase in solution pH produces a more positive reduction potential and we can get the same result according to Eq. (4).

To gain further insight on the electrochemical performance, EIS is used to evaluate the Cu²⁺ diffusion coefficient and the dynamic process on the interface of working electrodes. Figure 6 exhibits the typical EIS (presented in the form of the Nyquist plot) of the samples. The typical Nyquist plot includes a semicircle portion (known as capacity reactance arc) in the high-frequency range and a straight line in the low-frequency range. The high-frequency semicircle is related to the migration of the Cu²⁺ ions at the electrode/electrolyte interface and charge transfer process. The shape and semidiameter of the semicircle is linked to charge-transfer resistance at the interface between the electrolyte and the cathode [43–46]. A line in the low-frequency range is associated with the Warburg diffusion of the Cu²⁺ ions in the electrolyte [47]. To better understand the dynamic process on the interface of working electrodes, we plotted the electrical equivalent circuit. The equivalent circuit parameters are the reflection of EIS data. The simulation circuit and the simulation results are shown in the inset of Fig. 6. According to the impedance spectrum, we can calculate the equivalent circuit parameters. The calculated equivalent circuit parameters for the different pH values in solution are presented in Table 1.

Figure 6a shows a small capacitive arc in the high frequency range, indicating that the electrode process is carried out quickly. In addition, the capacitive arc is not a complete semicircle: its center is located in the fourth quadrant of the complex plane impedance, indicating there is a serious “dispersion effect.” In terms of experience, diffusion effect is usually caused by the inhomogeneous surface of the electrode [48]. The phenomenon indicates that Cu₂O film deposited on

Fig. 5 The linear sweep voltammogram of Cu_2O in an aqueous solution of 0.1 M sodium acetate and 0.02 M cupric acetate solutions with different pH values



FTO surface is very uneven. This is in agreement with the results observed in Fig. 3a.

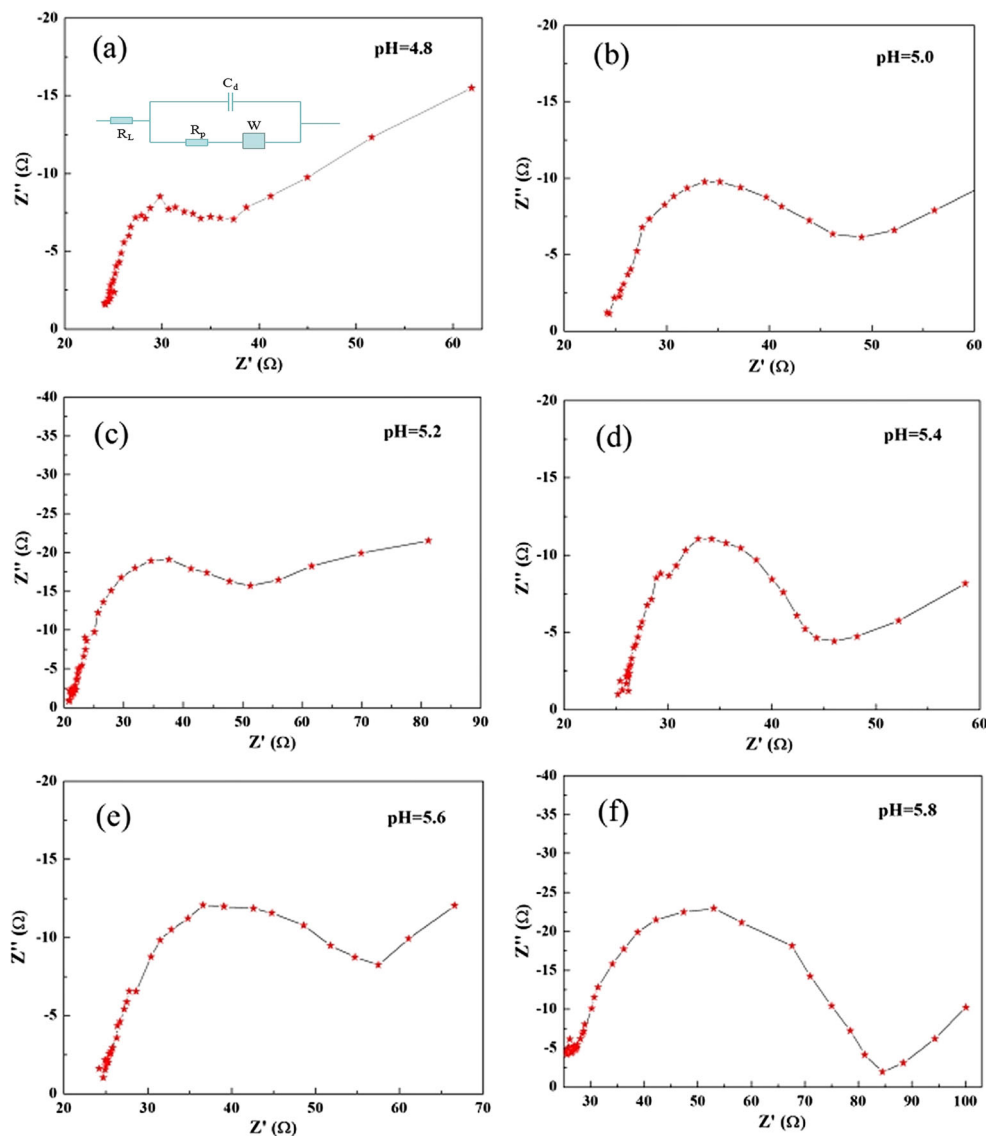
With increasing the pH from 5.0 to 5.8, EIS showed a new feature. As shown in Fig. 6b–f, the capacitive arc diameters in the high-frequency range gradually increase, which indicates that the charge transfer resistance R_p increases. This fact is consistent with the calculated equivalent circuit parameters in Table 1. We may safely draw the conclusion that electrochemical polarization increases, which is advantageous to the refinement of Cu_2O crystallization and improves Cu_2O adhesion strength on the FTO-coated glass [49]. In addition, the capacitive reactance arc in the high-frequency range is closer to semicircle, indicating a decrease of the dispersion effect. Hence, Cu_2O films in the electrode surface

become smooth, which is consistent with surface morphology observed in Fig. 3b–f. This means that it is easy to obtain a dense and a uniform Cu_2O thin film in a high pH solution.

Diffusion coefficient plays an important role in the analysis of the electrodeposited process of Cu_2O film. We can calculate the diffusion coefficient in different bath pH values by EIS. The inclined lines in the low-frequency range in Fig. 6 are attributed to a Warburg impedance. From the inclined lines in the Warburg region, the Cu^{2+} ion diffusion coefficient may be estimated using the following equation [49]:

$$D_0 = \frac{R^2 T^2}{2A^2 n^4 F^4 C_0^2 \sigma^2} \quad (6)$$

Fig. 6 The electrochemical impedance plot of Cu₂O in an electrolyte containing 0.1 M sodium acetate and 0.02 M cupric acetate with different pH values. *Inset:* the equivalent circuit model used in the fitting of the impedance data of the Cu₂O films, R_L = solution resistance, R_p = charge transfer resistance of the electrical double layer (EDL), W = Warburg impedance element, and C_d = double-layer capacitance



where R is the gas constant, T is the absolute temperature, A is the surface area of the cathode, n is the number of transferred electrons per molecule during deoxidization, F is the Faraday constant, C_0 is the Cu²⁺ ion concentration in electrode material, σ is the Warburg coefficient, and D_0 is the Cu²⁺ diffusion coefficient. In addition, σ is related to Z'' (imaginary part of impedance, reactive resistance), as shown in Eq. (7) [48–52].

$$Z'' = \sigma \omega^{-1/2} \tag{7}$$

Table 1 Parameters used for fitting the EIS data in Fig. 6

pH	4.8	5.0	5.2	5.4	5.6	5.8
R_L ($\Omega \cdot \text{cm}^2$)	24.41	25.68	21.43	26.42	25.28	25.87
R_p ($\Omega \cdot \text{cm}^2$)	10.27	18.54	25.84	26.72	28.01	63.56
ω^* (Hz)	18.6	8.8	4.18	6.59	8.82	7.34
C_d ($\text{mF} \cdot \text{cm}^{-2}$)	0.267	0.465	0.498	0.492	0.586	0.513

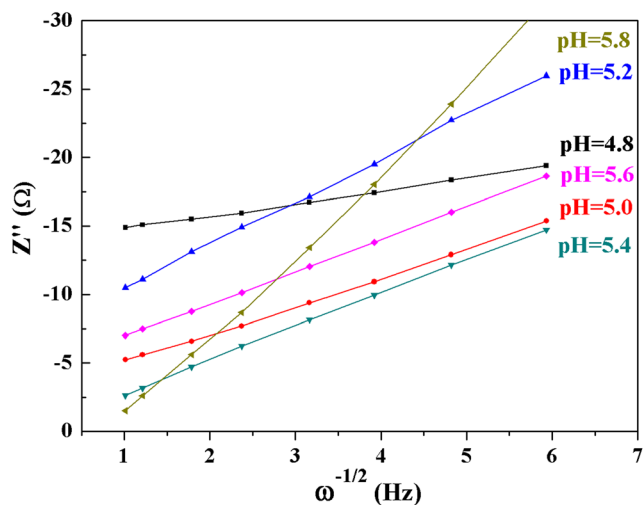


Fig. 7 Relationship between Z'' and square root of frequency ($\omega^{-1/2}$) in the low-frequency region, with different pH values

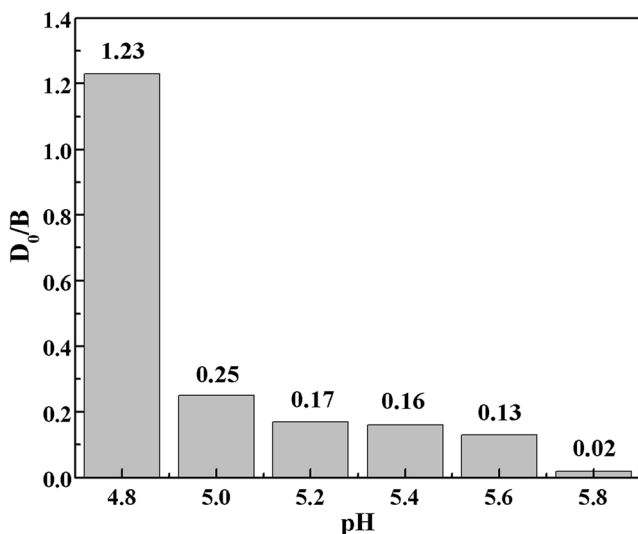


Fig. 8 D_0/B vs. pH of Cu_2O films prepared with different pH values, where B is a constant ($B = R^2T^2/2A^2n^4F^4C_0^2$)

Z'' and ω could be measured by the EIS. Therefore, the relationship between Z'' and reciprocal square root of frequency ($\omega^{-1/2}$) in the low-frequency region is shown in Fig. 7. From Eq. (7) and Fig. 7, the Warburg coefficient could be obtained.

Thus, the ratio of D_0/B could be obtained by Eq. (6), as is shown in Fig. 8, where B is a constant ($B = R^2T^2/2A^2n^4F^4C_0^2$).

Figure 8 shows the value of D_0/B decreases gradually with the increase of pH, which means that the diffusion coefficient D_0 also decreases. When the pH value is equal to 4.8, the diffusion coefficient D_0 is the largest and the transport capacity is the strongest. It is advantageous to fill Cu^{2+} ions into the clearance position. However, under the large pH (≥ 5.0) values, the Cu^{2+} ion diffusion transport speed becomes slow. And the rate of Cu_2O deposition is greater than that of the Cu^{2+} diffusion; it will form a depletion region around the

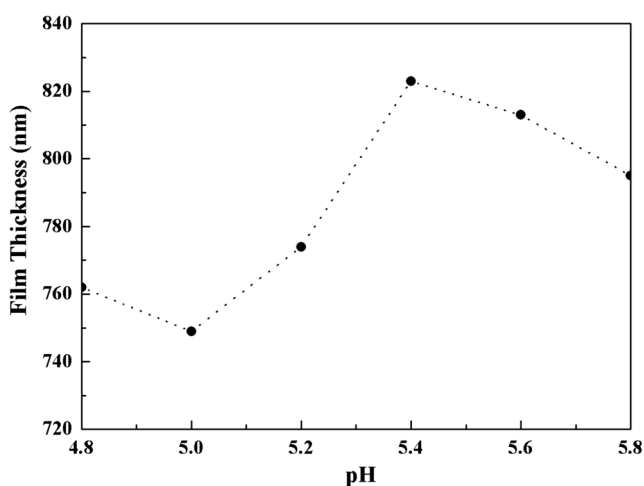


Fig. 9 Film thickness of Cu_2O as a function of bath pH

Cu_2O nuclei. So, the dendritic branching growth in electrodeposition can be induced and result in the formation of dendritic branching Cu_2O films.

Optical properties

Cu_2O is a typical direct band gap semiconductor. The optical band gap E_g was obtained from Eq. (8) [53, 54]:

$$(\alpha h\nu)^2 = A(h\nu - E_g) \quad (8)$$

Here, α is the absorption coefficient, A is a constant, h is the discrete photon energy, and E_g is the band gap energy. The absorption coefficient α can be obtained by the following formula:

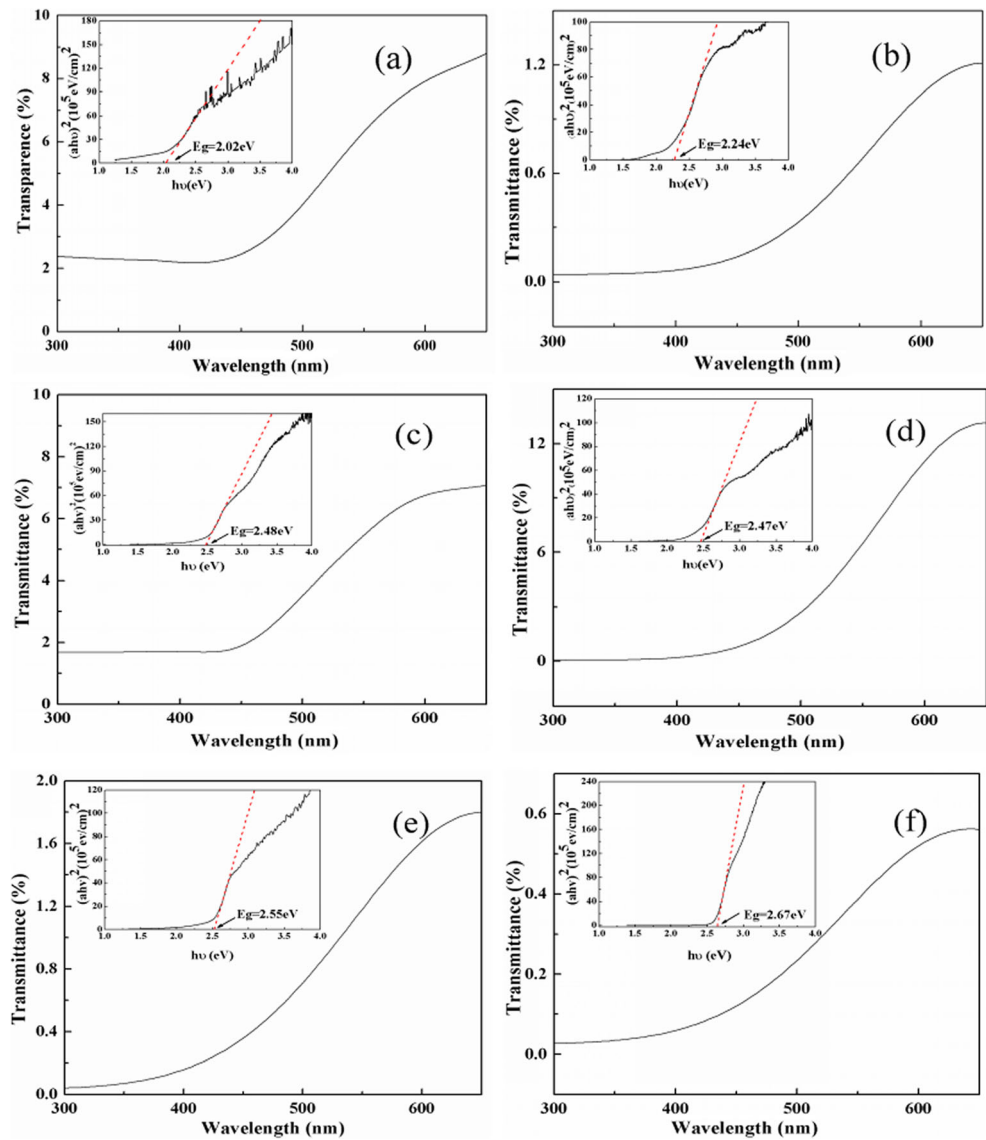
$$\alpha = (d^{-1}) \ln(T^{-1}) \quad (9)$$

where T is the transmittance and d is thickness of film, respectively. The thickness of Cu_2O films is shown in Fig. 9.

Figure 10 illustrates the transmittance spectrum of the Cu_2O film grown on FTO glass under the conditions of different pH 4.8, 5.0, 5.2, 5.4, 5.6, and 5.8. It can be seen that all films show a low transmission (smaller than 15 %) in the wavelength between 300 and 650 nm. Therefore, this phenomenon demonstrates a strong adsorption in the wavelength range from 300 to 650 nm, which is the characteristic absorption of Cu_2O .

The band gap E_g is obtained by extrapolation the linear section of the plot of $(\alpha h)^2$ vs. h , and the estimated direct band gaps of Cu_2O films are listed in Table 2. It can be found that the absorption edges show redshift then blueshift in comparison with that of bulk Cu_2O (2.09 eV), with the increasing of pH. The optical band gap of semiconductors could be severely affected by the defects, disorder at the grain boundaries, crystallinity, as well as the stress of the crystals, which could decrease the energy band gap with the presence of tensile stress in crystals [55–57]. According to the analysis of XRD, tensile stress existed in the crystals when the pH value was 4.8. It resulted in the band gap smaller according to the theory of quantum mechanics periodic potential [58, 59]. Therefore, it generated redshift in the spectrum of the Cu_2O film when the pH value was 4.8. The band gaps of the samples for pH value of 5.0, 5.2, 5.4, 5.6, and 5.8 shows blueshift. The possible reason is the following. The crystalline lattice of Cu_2O became shrunk, resulting in the decrease of the distance between the atoms, which indicated Cu_2O crystals were under compressive stress. In this case, blueshift phenomenon would appear according to the theory of quantum mechanics periodic potential [58].

Fig. 10 $(\alpha h\nu)^2$ vs. photon energy ($h\nu$) of Cu₂O films prepared with different pH values for samples **a** 4.8, **b** 5.0, **c** 5.2, **d** 5.4, **e** 5.6, and **f** 5.8



Conclusions

In summary, Cu₂O with different morphologies and sizes were easily obtained on fluorine-doped tin oxide (FTO) covered glass substrates by potentiostatic deposition. LSV showed that reduction potential slightly increased with increasing pH. The impedance spectra indicated that the electrochemical

polarization was become large and diffusion coefficient became small with increasing pH. Thus, we can get different morphologies and excellent performance of Cu₂O thin films by changing the pH of the solution. With controlling the pH, the optical transmittance of the Cu₂O was under 15 % in the wavelength range of 300–650 nm, and the optical band gaps of Cu₂O thin films calculated from the transmission spectra were changing from 2.06–2.84 eV.

Table 2 Estimated optical band gaps from $(\alpha h)^2$ vs. photon energy (h) plots of prepared Cu₂O films at different pH values

Bath pH	4.8	5.0	5.2	5.4	5.6	5.8
Band gap (eV)	2.02	2.24	2.48	2.47	2.55	2.67

Acknowledgments The authors thank the ‘863’ project of China (No. 2009AA03Z427) for providing research grant.

References

- Orel ZC, Anzlovar A, Drazic G, Zigon M (2007) Cuprous oxide nanowires prepared by an additive-free polyol process. *Cryst Growth Des* 7:453–458
- Kuo CH, Huang MH (2010) Morphologically controlled synthesis of Cu₂O nanocrystals and their properties. *Nano Today* 5:106–116
- Park JC, Kim J, Kwon H, Song H (2009) Gram-scale synthesis of Cu₂O nanocubes and subsequent oxidation to CuO hollow nanostructures for lithium-ion battery anode materials. *Adv Mater* 21:803–807
- Miyake M, Chen YC, Braun PV, Wiltzius P (2009) Fabrication of three-dimensional photonic crystals using multibeam interference lithography and electrodeposition. *Adv Mater* 21:3012–3015
- Huang L, Peng F, Wang HJ, HaO Y, Li Z (2009) Preparation and characterization of Cu₂O/TiO₂ nano-nano heterostructure photocatalysts. *Catal Commun* 10:1839–1843
- Wei HM, Gong HB, Chen L, Zi M, Cao BQ (2012) Photovoltaic efficiency enhancement of Cu₂O solar cells achieved by controlling homojunction orientation and surface microstructure. *J Phys Chem C* 116:10510–10515
- Paracchino A, Brauer JC, Moser JE, Thimsen E, Graetzel M (2012) Synthesis and characterization of high-photoactivity electrodeposited Cu₂O solar absorber by photoelectrochemistry and ultrafast spectroscopy. *J Phys Chem C* 116:7341–7350
- Oshero A, Zhu CQ, Panzer MJ (2013) Role of solution chemistry in determining the morphology and photoconductivity of electrodeposited cuprous oxide films. *Chem Mater* 25:692–698
- McShane CM, Siripala WP, Choi KS (2010) Effect of junction morphology on the performance of polycrystalline Cu₂O homojunction solar cells. *J Phys Chem Lett* 1:2666–2670
- Cui JB, Gibson UJ (2010) A simple two-step electrodeposition of Cu₂O/ZnO nanopillar solar cells. *J Phys Chem C* 114:6408–6412
- Mittiga A, Salza E, Sarto F, Tucci M, Vasanthi R (2006) Heterojunction solar cell with 2 % efficiency based on a Cu₂O substrate. *Appl Phys Lett* 88:163502 (2pp)
- Lamberti A, Destro M, Bianco S, Quaglio M, Chiodoni A, Pirri CF, Gerbaldi C (2012) Facile fabrication of cuprous oxide nanocomposite anode films for flexible Li-ion batteries via thermal oxidation. *Electrochim Acta* 86:323–329
- Bergerot L, Jiménez C, Pluchery OC, Rapenne L, Deschanvres JL (2015) Growth and characterization of Sr-doped Cu₂O thin films deposited by metalorganic chemical vapor deposition. *Phys Status Solidi A* 212:1735–1741
- Chu CL, Lu HC, Lo CY, Lai CY, Wang YH (2009) Physical properties of copper oxide thin films prepared by dc reactive magnetron sputtering under different oxygen partial pressures. *Physica B* 404:4831–4834
- Xu HL, Wang WZ (2007) Template synthesis of multishelled Cu₂O hollow spheres with a single-crystalline shell wall. *Angew Chem Int Ed* 46:1489–1492
- Lu CH, Qi LM, Yang JH, Wang XY, Zhang DY, Xie JL, Ma JM (2005) One-pot synthesis of octahedral Cu₂O nanocages via a catalytic solution route. *Adv Mater* 17:2562–2567
- Huang L, Peng F, Yu H, Wang HJ (2009) Preparation of cuprous oxides with different sizes and their behaviors of adsorption, visible-light driven photocatalysis and photocorrosion. *Solid State Sci* 11:129–138
- Ai ZH, Zhang LZ, Lee SC, Ho W (2009) Interfacial hydrothermal synthesis of Cu@Cu₂O core-shell microspheres with enhanced visible-light-driven photocatalytic activity. *J Phys Chem C* 113:20896–20902
- Siegfried MJ, Choi KS (2005) Directing the architecture of cuprous oxide crystals during electrochemical growth. *Angew Chem Int Ed* 44:3218–3223
- Siegfried MJ, Choi KS (2006) Elucidating the effect of additives on the growth and stability of Cu₂O surfaces via shape transformation of pre-grown crystals. *J Am Chem Soc* 128:10356–10357
- Paracchino A, Laporte V, Sivula K, Grätzel M, Thimsen E (2011) Highly active oxide photocathode for photoelectrochemical water reduction. *Nat Mater* 10:456–461
- Liau LCK, Lin YC, Peng YJ (2013) Fabrication pathways of p-n Cu₂O homojunction films by electrochemical deposition processing. *J Phys Chem C* 117:26426–26431
- Jeong YS, Kim H, Lee HS (2013) Growth and characterization of p-Cu₂O/n-ZnO nanorod heterojunctions prepared by a two-step potentiostatic method. *J Alloys Compd* 573:163–169
- Wei HM, Gong HB, Wang YZ, Hu XL, Chen L, Xu HY, Liu P, Cao BQ (2011) Three kinds of Cu₂O/ZnO heterostructure solar cells fabricated with electrochemical deposition and their structure-related photovoltaic properties. *CrystEngComm* 13:6065–6070
- Li Q, Xu MM, Fan HQ, Wang HR, Peng BL, Long CB, Zhai YC (2013) Electrical charge conductivity behavior of electrodeposited Cu₂O/ZnO heterojunction thin films on PET flexible substrates by impedance spectroscopy analysis. *J Mater Sci* 48:3334–3340
- Sun F, Guo YP, Song WB, Zhao JZ, Tang LQ, Wang ZC (2007) Morphological control of Cu₂O micro-nanostructure film by electrodeposition. *J Cryst Growth* 304:425–429
- Tang YW, Chen ZG, Jia ZJ, Zhang LS, Li JL (2005) Electrodeposition and characterization of nanocrystalline cuprous oxide thin films on TiO₂ films. *Mater Lett* 59:434–438
- Ghadimkhani G, de Tacconi NR, Chanmanee W, Janaky C, Rajeshwar K (2013) Efficient solar photoelectrosynthesis of methanol from carbon dioxide using hybrid CuO-Cu₂O semiconductor nanorod arrays. *Chem Commun* 49:1297–1299
- Shao F, Sun J, Gao L, Luo JQ, Liu YQ, Yang SW (2012) High efficiency semiconductor-liquid junction solar cells based on Cu/Cu₂O. *Adv Funct Mater* 22:3907–3913
- Liu XM, Zhou YC (2005) Electrochemical deposition and characterization of Cu₂O nanowires. *Appl Phys A Mater Sci Process* 81:685–689
- Bijani S, Martnez L, Gabas M, Dalchiale EA, Ramos-Barrado J-R (2009) Low-temperature electrodeposition of Cu₂O thin films: modulation of micro-nanostructure by modifying the applied potential and electrolytic bath pH. *J Phys Chem C* 113:19482–19487
- Bao M, Wang D, Liu SY, Kuang LL, Sun J, Wang F, Wen YX (2012) Electrodeposition and electrocatalytic activity of Cu₂O film on stainless steel substrate. *Appl Surf Sci* 258:8008–8014
- Zhao WY, Fu WY, Yang HB, Tian CJ, Li MH, Li YX, Zhang L, Sui YM, Zhou XM, Chen H, Zou GT (2011) Electrodeposition of Cu₂O films and their photoelectrochemical properties. *CrystEngComm* 13:2871–2877
- Xue JB, Liang W, Liu XG, Shen QQ, Xu BS (2012) Crystallization behavior and formation mechanism of dendrite Cu₂O crystals. *CrystEngComm* 14:8017–8022
- Pourbaix M (1974) Atlas of electrochemical equilibria in aqueous solutions. National Association of Corrosion Engineers, Houston, pp. 384–392
- McShane CM, Choi KS (2009) Photocurrent enhancement of n-type Cu₂O electrodes achieved by controlling dendritic branching growth. *J Am Chem Soc* 131:2561–2569
- Siegfried MJ, Choi K-S (2008) Elucidation of an overpotential-limited branching phenomenon observed during the electrocrystallization of cuprous oxide. *Angew Chem Int Ed* 47:368–372
- Huang L, Peng F, Wang HJ, Yu H, Geng W, Yang J, Zhang SQ, Zhao HJ (2011) Controlled synthesis of octahedral Cu₂O on TiO₂ nanotube arrays by electrochemical deposition. *Mater Chem Phys* 130:316–322
- Han K, Kang F, Han XF, Tao M (2012) Enhanced crystal grain size by bromine doping in electrodeposited Cu₂O. *Thin Solid Films* 520:5239–5244

40. Lopez CM, Choi K-S (2006) Electrochemical synthesis of dendritic zinc films composed of systematically varying motif crystals. *Langmuir* 22:10625–10629
41. Brady RM, Bal RC (1984) Fractal growth of copper electrodeposits. *Nature* 309:225–229
42. Wong EM, Searson PC (1999) ZnO quantum particle thin films fabricated by electrophoretic deposition. *Appl Phys Lett* 74:2939–2941
43. Huang S, Luo WJ, Zou ZG (2013) Band positions and photoelectrochemical properties of $\text{Cu}_2\text{ZnSnS}_4$ thin films by the ultrasonic spray pyrolysis method. *J Phys D Appl Phys* 46: 235108 (6pp)
44. Li LX, Tang XC, Liua HT, Qu Y, Lua ZG (2010) Morphological solution for enhancement of electrochemical kinetic performance of LiFePO_4 . *Electrochim Acta* 56:995–999
45. Wang L, Wang HB, Liu ZH, Xiao C, Dong SM, Han PX, Zhang ZY, Zhang XY, Bi CF, Cui GL (2010) A facile method of preparing mixed conducting LiFePO_4 /graphene composites for lithium-ion batteries. *Solid State Ionics* 181:1685–1689
46. Wang YR, Yang YF, Yang YB, Shao HX (2010) Enhanced electrochemical performance of unique morphological LiMnPO_4 /C cathode material prepared by solvothermal method. *Solid State Commun* 150:81–85
47. Pasquale MA, Gassa LM, Arvia AJ (2008) Copper electrodeposition from an acidic plating bath containing accelerating and inhibiting organic additives. *Electrochim Acta* 53:5891–5904
48. Jia Z, Dai CS, Chen L (2006) Electrochemical measurement methods. Chemical industry press, Peking, pp. 170–173
49. Zhang JQ (2011) Electrochemical measurement technology. Chemical industry press, Peking, pp. 220–225
50. Bard AJ, Faulkner LR (2001) Electrochemical methods: fundamentals and applications, 2nd edn. Wiley, New York, pp. 381–385
51. Hu HL (2007) Electrochemical measurement. National Defence Industry Press, Peking, pp. 212–229
52. Zhou YK, Wang J, Hu YY, O'Hayreb R, Shao ZP (2010) A porous LiFePO_4 and carbon nanotube composite. *Chem Commun* 46: 7151–7153
53. Tauc J, Mentha A (1972) States in the gap. *J Non-Cryst Solids* 8(10): 569–585
54. Liu YL, Liu YC, Mu R, Yang H, Shao CL, Zhang JY, Lu YM, Shen DZ, Fan XW (2005) The structural and optical properties of Cu_2O films electrodeposited on different substrates. *Semicond Sci Technol* 20:44–49
55. Dow JD, Redfield D (1972) Toward a unified theory of Urbach's rules and exponential absorption edges. *Phys Rev B* 5:594–610
56. Revathi N, Prathap P, Subbaiah YPV, Reddy KTR (2008) Substrate temperature dependent physical properties of In_2S_3 films. *J Phys D Appl Phys* 41:155404 (10pp)
57. Dong GB, Zhang M, Wang M, Li YZ, Li CR, Li H, Huang AP, Yan H (2012) Effect of substrate temperature on the structure and properties of Cu_2O thin films. *J Synth Cryst* 41:457–460
58. Qiao ZG (2005) Semiconductor physics. Zhejiang university press, Zhejiang, pp. 56–64
59. Kittel C (1996) Introduction to solid state physics. Wiley, New York, pp. 121–125